

Sodium Biphenyl as Anolyte for Sodium–Seawater Batteries

Yongil Kim, Jaeho Jung, Hyein Yu, Guk-Tae Kim, Dasong Jeong, Dominic Bresser, Seok Ju Kang,* Youngsik Kim,* and Stefano Passerini*

Sodium-based battery systems have recently attracted increasing research interest due to the abundant resources employed. Among various material candidates for the negative electrode, sodium metal provides the highest capacity of theoretically 1165 mAh g⁻¹ and a very low redox potential of -2.71 versus the standard hydrogen electrode. However, the high reactivity of sodium metal toward the commonly used electrolytes results in severe side reactions, including the evolution of gaseous decomposition products, and, in addition, the risk of dendritic sodium growth, potentially causing a disastrous short circuit of the cell. Herein, the use of sodium biphenyl (Na-BP) as anolyte for the Na–seawater batteries (Na–SWB) is investigated. The catholyte for the open-structured positive electrode is natural seawater with sodium cations dissolved therein. Remarkably, the significant electronic and ionic conductivities of the Na-BP anolyte enable a low overpotential for the sodium deposition upon charge, allowing for high capacity and excellent capacity retention for 80 cycles in full Na–SWB. Additionally, the Na-BP anolyte suppresses gas evolution and dendrite growth by forming a homogeneous surface layer on the metallic negative electrode.

sources like solar and wind.^[1] Due to the highly intermittent nature of these latter, however, efficient energy storage technologies are essential for the successful transition toward a sustainable future.^[2] Among these, electrical and electrochemical energy storage systems are the most efficient ones, while the latter, i.e., batteries, are simultaneously providing suitable energy densities and negligible self-discharge.^[3] In this regard, sodium-based battery technologies are very attractive alternatives,^[4] especially when employing highly abundant sodium-containing cathode materials as, for instance, seawater—also referred to as seawater batteries (SWBs).^[5] Unlike seawater batteries researched in the past,^[5d–f] the system introduced in this research is a secondary battery, i.e., it can be recharged, showing long life and high operating voltage. In such configuration, the positive electrode provides an

essentially unlimited amount of sodium, if a continuous flow of seawater is ensured in an “open system.”^[6]

The electrochemical processes occurring in these cells are

	Negative electrode	Positive electrode
Charge:	$\text{Na}^+ + (\text{H}) + \text{e}^- \rightarrow \text{Na}(\text{H})$	$\text{NaCl}(\text{aq}) \rightarrow \text{Na}^+ + 1/2\text{Cl}_2(\text{g}) + \text{e}^-$ $\text{NaCl}(\text{aq}) + 2\text{OH}^-(\text{aq}) \rightarrow \text{Na}^+ + \text{ClO}^- + \text{H}_2\text{O} + 2\text{e}^-$ $2\text{OH}^-(\text{aq}) \rightarrow \text{H}_2\text{O} + 1/2\text{O}_2(\text{g}) + 2\text{e}^-$
Discharge:	$\text{Na}(\text{H}) \rightarrow \text{Na}^+ + \text{e}^-$	$2\text{Na}^+ + \text{H}_2\text{O} + 1/2\text{O}_2(\text{g}) + 2\text{e}^- \rightarrow 2\text{NaOH}(\text{aq})$

The capacity of each battery cell is limited by the (reversible) sodium storage capability of the negative electrode—at least if common host structures (H) for sodium cations are employed, such as hard carbons. Differently, the plating of metallic sodium would be limited only by the available volume at the negative electrode and, in addition, provide the highest possible cell voltage, i.e., energy density, thanks to its low redox potential (-2.71 V vs the standard hydrogen electrode) and high theoretical capacity (1165 mAh g⁻¹).^[7] Nevertheless, the high reactivity and the extensive volume changes upon plating and stripping (i.e., charge and discharge) of the Na metal electrode result in a rather unstable solid electrolyte interphase (SEI). This is accompanied by an ongoing electrolyte consumption and evolution of gaseous decomposition products. Additionally, according to a recent research, the higher electronic conductivity of solid electrolytes with respect to liquid electrolytes causes a lower overpotential and a severe potential fluctuation near heterogeneities


1. Introduction

The increasing energy demand and the consequently increasing utilization of fossil fuels comes with continuously rising concerns about environmental pollution and catastrophic climate change. Hence, it is indispensable to substantially reduce, ideally avoid, the energy supply by these unsustainable resources and make use of renewable energy

Dr. Y. Kim, Dr. G.-T. Kim, Dr. D. Bresser, Prof. S. Passerini
Helmholtz Institute Ulm (HIU)
Helmholtzstrasse 11, Ulm 89081, Germany

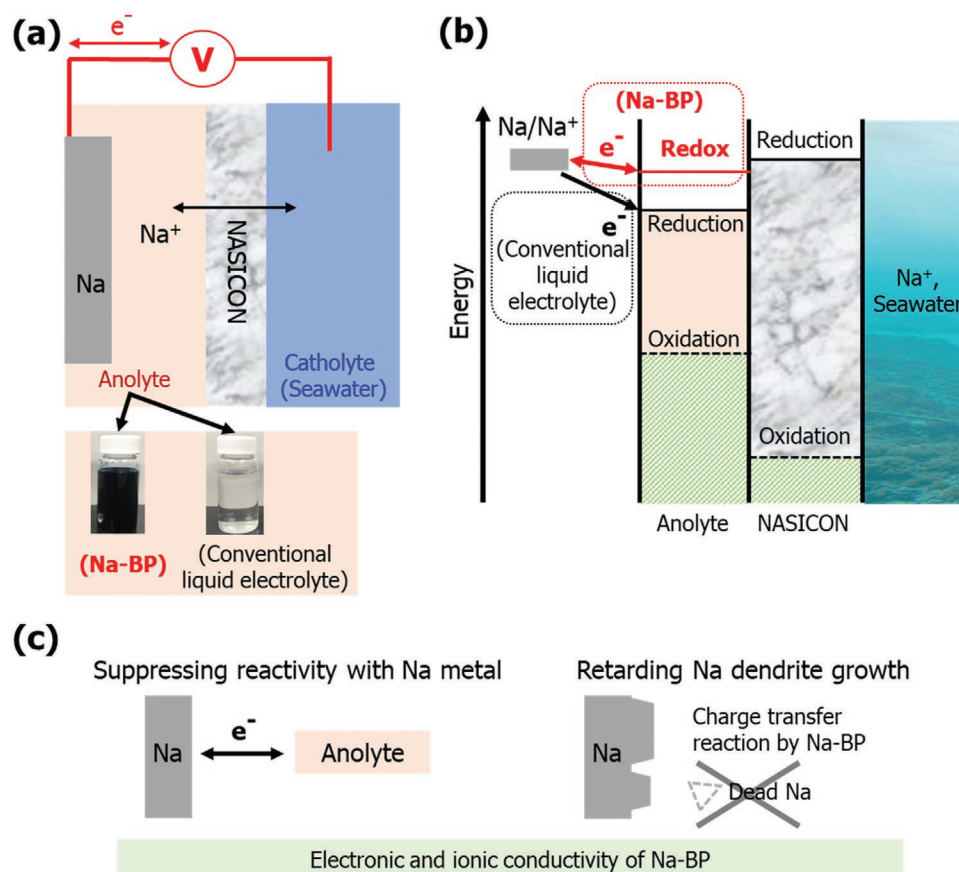
Dr. Y. Kim, Dr. G.-T. Kim, Dr. D. Bresser, Prof. S. Passerini
Karlsruhe Institute of Technology (KIT)
P. O. Box 3640, Karlsruhe 76021, Germany
E-mail: stefano.passerini@kit.edu

J. Jung, H. Yu, D. Jeong, Prof. S. J. Kang, Prof. Y. Kim
School of Energy and Chemical Engineering
Ulsan National Institute of Science and Technology (UNIST)
UNIST-gil 50, Ulsan 44919, Republic of Korea
E-mail: sjkang@unist.ac.kr; ykim@unist.ac.kr

 The ORCID identification number(s) for the author(s) of this article can be found under <https://doi.org/10.1002/adfm.202001249>.

© 2020 The Authors. Published by WILEY-VCH Verlag GmbH & Co. KGaA, Weinheim. This is an open access article under the terms of the Creative Commons Attribution-NonCommercial-NoDerivs License, which permits use and distribution in any medium, provided the original work is properly cited, the use is non-commercial and no modifications or adaptations are made.

DOI: 10.1002/adfm.202001249



Scheme 1. Illustrative overview of the general concept when employing Na-BP as anolyte in SWBs. a) The general cell setup with two photographs showing the Na-BP anolyte solution in comparison with a conventional liquid electrolyte. b) The energy diagram of the multilayer electrolyte SWB system. c) The anticipated beneficial impact on the stability of the sodium metal anode when using the Na-BP anolyte.

during cycling, resulting in a greater driving force for dendritic metal formation.^[8] The formation of gaseous products and the severe risk of dendrite growth pose substantial challenges toward the commercialization of SWBs employing metallic sodium.^[4b] In this work, it is shown as the use of biphenyl as anolyte solve the problem of sodium metal anodes by spontaneously forming Na-biphenyl (Na-BP). This compound has been already studied as presodiation agent^[9] and liquid anode material for sodium-based batteries,^[10] providing simultaneously suitable electronic and ionic conductivity.^[10a] Na-BP is indeed expected to reduce overpotential at the anolyte–Na interface and, maintaining a high homogeneity within the anolyte, potential fluctuations at the Na metal surface, unlike the solid electrolyte.

Herein, we take benefit of these advantageous properties and the multilayer electrolyte design of SWBs with a NASICON ($\text{Na}_3\text{Zr}_2\text{Si}_2\text{PO}_{12}$) solid electrolyte layer, physically separating the negative and positive cell compartments, by employing Na-BP as anolyte for sodium metal anodes (see **Scheme 1a**). Because of its high reversible and low redox potential (vs Na/Na^+), Na-BP can act as redox mediator, suppressing the electrolyte decomposition at the sodium metal anode (**Scheme 1b**). As such, the Na-BP anolyte simultaneously contributes to the reversible sodium cation storage and enables the homogeneous, low-overpotential sodium metal deposition. As a result, the introduction of low-

cost biphenyl (compared to common salts for liquid electrolytes) allows for suppressing the continuous electrolyte decomposition and mitigates sodium dendrite growth (**Scheme 1c**).

2. Results and Discussion

The electrochemical performance of the $\text{Na}_{\text{sat}}\text{-}1\text{ M BP}$ -diethylene glycol dimethyl ether (DEGDME) solution (later on defined as Na-BP) have been investigated in two-electrode half-cells, hosted in coin-cell cases. In these cells, a NASICON solid electrolyte layer was employed to physically separate Na-BP, acting as active material at the positive electrode, and the sodium metal acting as the negative electrode (see **Figure 1a** for the cell setup). A photograph of Na-BP in comparison with a more conventional, sodium(-ion) battery electrolyte, i.e., 1 M NaOTF in tetraethylene glycol dimethyl ether (TEGDME), is presented in **Figure S1a** of the Supporting Information, revealing a transparent colorless liquid for the latter and a dark blue liquid for Na-BP. As apparent from **Figure 1b** and **Figure S1b** (Supporting Information), no capacity is observed upon the first discharge, i.e., formation of Na-BP, at 0.25 mA cm^{-2} due to the already complete chemical transformation of biphenyl into Na-BP (see the corresponding description in the Experimental Section). For

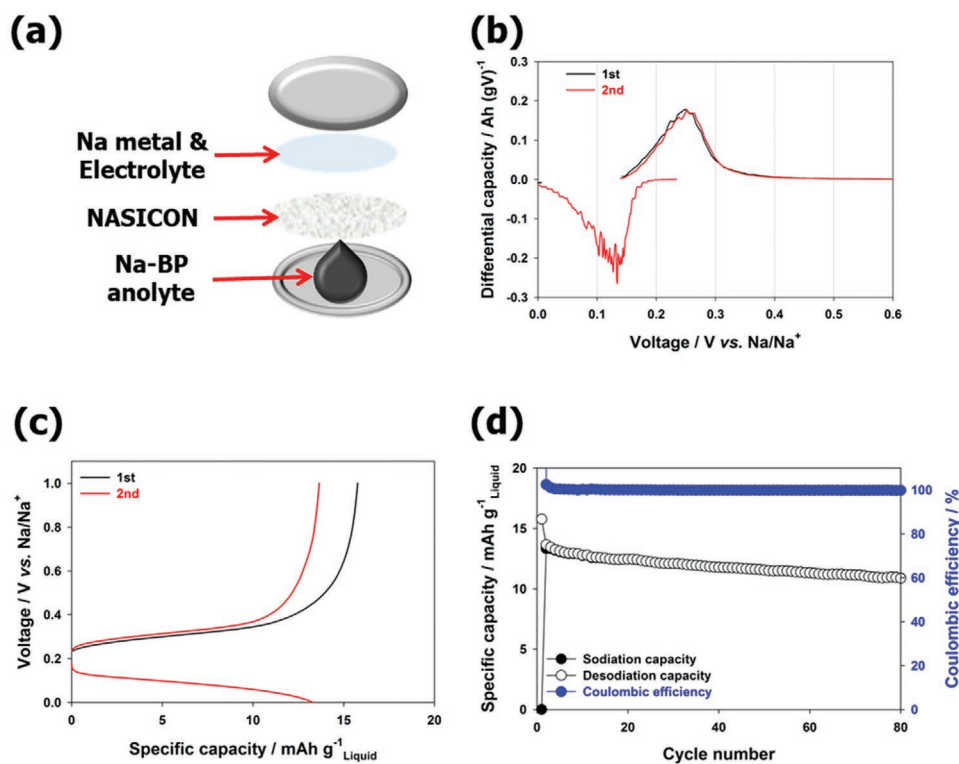


Figure 1. a) Schematic illustration of the cell setup for the electrochemical characterization of Na-BP as liquid active material in half-cell configuration with a sodium metal counter electrode and a layer of NASICON as solid electrolyte to physically separate the two electrodes. b) Plot of the differential capacity (dQ/dV) as a function of the cell voltage when applying a current density of 0.25 mA cm^{-2} . c) Dis-/charge profiles for the 1st and 2nd cycle when subjecting such half-cells to a current density of 0.5 mA cm^{-2} (cut-off potentials: 0.0 and 1.0 V vs Na/Na⁺) and d) the plot of the specific capacity versus cycle number for 80 cycles.

the subsequent charge, i.e., desodiation, a capacity of 18 mAh g^{-1} is obtained based on total weight of the liquid. For the 2nd cycle, the Na-BP anolyte shows a capacity of $17.4 \text{ mAh g}^{-1}_{\text{Na-BP}}$ for both the sodiation and desodiation, revealing an excellent charge reversibility. This is also accompanied by a good voltage reversibility with average discharge and charge voltages of about 0.13 and 0.25 V, respectively (Figure 1b; Figure S1b, Supporting Information). In fact, the achieved capacity values are slightly lower than the theoretical capacity of $30 \text{ mAh g}^{-1}_{\text{Na-BP}}$ (with a density of 0.98 g mL^{-1} , which means that the volumetric theoretical capacity is about $29.4 \text{ Ah L}^{-1}_{\text{Na-BP}}$), indicating that the utilization of Na-BP is limited, at least at such C rate, presumably due to the limited electronic conductivity and required contact to the current collector for the electron transfer. Nonetheless, the sodium utilization of around 58% is, indeed, remarkable. When doubling the current density to 0.5 mA cm^{-2} , the average sodiation and desodiation potential increase to about 0.1 and 0.3 V, respectively, while the utilization decreases to about 48% of the theoretical value (Figure 1c). Upon continuous cycling (Figure 1d) the capacity shows a slight fading, but the average coulombic efficiency is rather high with around 99.8% considering that a sodium metal counter electrode is used.

Following this promising performance in half-cells, we employed Na-BP as anolyte in seawater full-cells (see Figure 2a for the cell setup). Nickel foam and carbon felt were used as current collectors for the anode and the cathode, respectively. The dis-/charge profiles upon the 1st and 2nd cycles for the galva-

nostatically cycled cell with a current density of 0.5 mA cm^{-2} are presented in Figure 2b. Upon the initial discharge, i.e., desodiation of the anolyte (Na-BP), the cell provides a specific capacity of $20.8 \text{ mAh g}^{-1}_{\text{Na-BP}}$ along a very flat voltage plateau at around 2.61 V. A rather similarly flat voltage plateau at about 2.6 V is observed also during the 2nd discharge. On the other hand, the charge step during the 1st and 2nd cycle shows an average charge voltage of 3.61 V. For the charge steps, the capacity was fixed to the initially obtained value (i.e., $20.8 \text{ mAh g}^{-1}_{\text{Na-BP}}$) and kept constant throughout the following galvanostatic cycling (see also Figure 2c). After 80 cycles, the seawater-battery full-cell provides a capacity retention of 94.2% with an average coulombic efficiency of 93.1%. Interestingly, it is higher for the initial 30 cycles, before it slightly drops due to a lower discharge capacity, though remaining rather constant afterward.

To comprehensively understand the underlying reaction mechanism(s) in this rather complex system, we designed a set of complementary experiments using different analysis techniques. In a first step, we determined the ionic and electronic conductivity of Na-BP using a conductivity meter, revealing a value of about $5.7 \times 10^{-3} \text{ S cm}^{-1}$ at room temperature for the sum of the two contributions. To separate the two contributions, we utilized the isothermal transient ionic current (ITIC) method.^[11] For this, we assembled suitable electrochemical cells with two stainless steel blocking electrodes, sandwiching the Na-BP anolyte as schematized in Figure S2a of the Supporting Information. A constant voltage of 0.1 V was applied

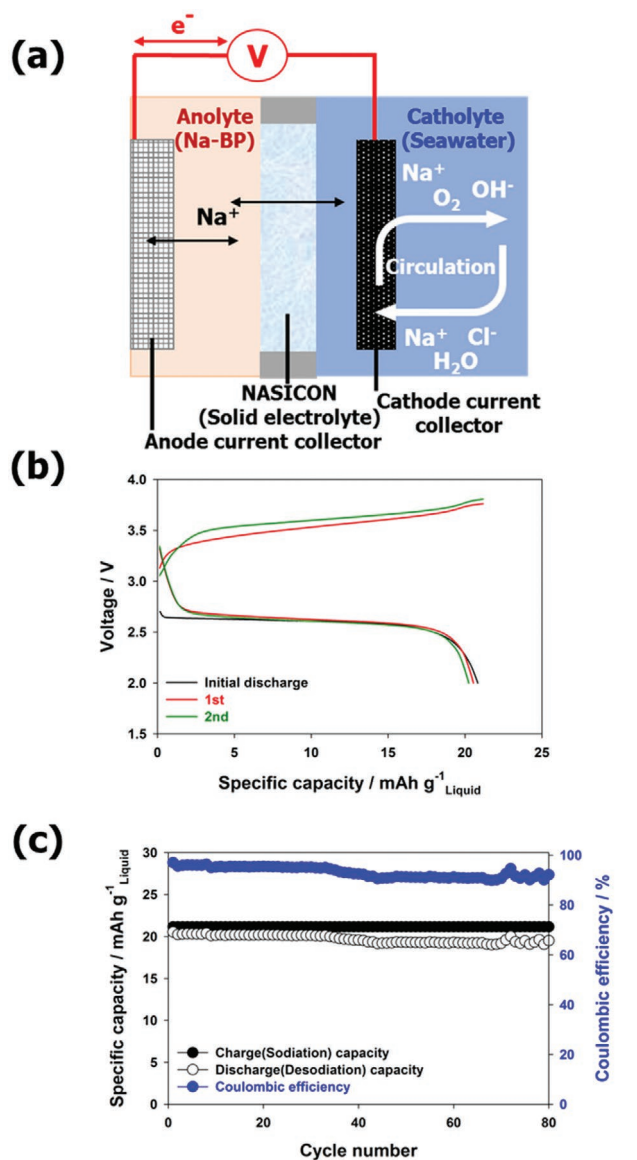


Figure 2. a) Schematic illustration of the cell setup for seawater-battery full-cells employing the Na-BP solution as anolyte and seawater as catholyte. The electrodes are physically separated by a NASICON solid electrolyte layer and nickel foam and carbon felt are serving as current collector for the anode and cathode, respectively. b) Dis-/charge profiles of the initial discharge (in black) as well as the 1st (in red) and 2nd (in green) galvanostatic cycle, applying a current density of 0.5 mA cm⁻². c) Plot of the specific capacity for the anode based on the total weight of the Na-BP solution versus the cycle number for the continuous galvanostatic cycling.

and the evolving current was recorded for 1 h (Figure 3a). The ionic and electronic conductivity are then calculated by using Equation (1), where $J(t)$ is the current density as a function of time, σ_{dc,e^-} is the electronic conductivity, σ_{dc,Na^+} is the ionic conductivity, U is the applied voltage, μ_{Na^+} is the sodium-ion mobility, and t is the time

$$J(t) = \frac{\sigma_{dc,e^-} U}{L} + \frac{\sigma_{dc,Na^+} U}{L} \exp\left(-\frac{\mu_{Na^+} U}{L^2} t\right) \quad (1)$$

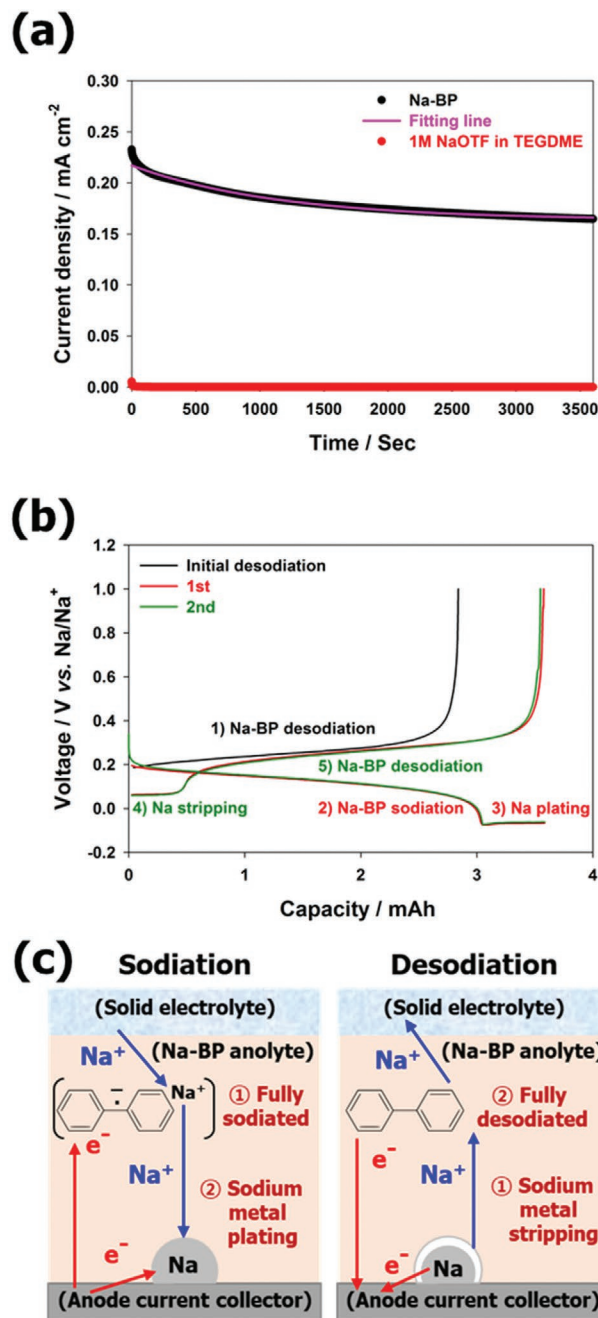


Figure 3. a) Plot of the electronic and ionic conductivity of Na_{sat}-1 m BP-DEGDME and 1 m NaOTF in TEGDME by employing the ITIC method. b) Dis-/charge profiles for the galvanostatic “over(de)sodiation” of Na-BP half-cells employing Ni foam as anode current collector (current density: 0.25 mA cm⁻²). c) Schematic illustration of the charge and discharge process employing Na-BP in DEGDME as anolyte.

Following this calculation, the ionic conductivity of Na-BP is $1.39 \times 10^{-3} \text{ S cm}^{-1}$ and the electronic conductivity is $4.26 \times 10^{-3} \text{ S cm}^{-1}$. These conductivities are sufficiently high to ensure a suitable sodium cation transport and electron transfer for its application in a battery. The sum of these two values (i.e., more than $5.65 \times 10^{-3} \text{ S cm}^{-1}$) is in very good agreement with the value determined by the conductivity meter, confirming the

general suitability of this approach.^[10a] For comparison, the conventional liquid electrolyte (1 M NaOTf in TEGDME) was also studied.^[12] Obviously, its electronic conductivity was found to be negligible, using the ITIC method (see Figure 3a). The ionic conductivity determined with the conductivity meter was found to be $0.965 \times 10^{-3} \text{ S cm}^{-1}$, i.e., in good agreement with the value determined by electrochemical impedance spectroscopy (EIS) ($0.904 \times 10^{-3} \text{ S cm}^{-1}$ see Figure S2b, Supporting Information). Interestingly, the ionic conductivity of the conventional liquid electrolyte is slightly lower than that of Na-BP.

In a next step, the potential use of Na-BP to assemble cells without employing Na metal (also called sodium metal-free cells) was investigated. For the preliminary investigation, cells were made according to the (half-)cell setup described in Figure 1a. In these cells, only Ni foam was used to serve as current collector on the Na-BP compartment (although Na-PB acts as the positive electrode in these cells, it is still referred to as the anolyte). Initially, Na-BP was desodiated at 0.25 mA cm⁻² up to 1.0 V in order to determine the capacity delivered from the Na-BP in its initial state. This test revealed a total capacity of 2.8 mAh (i.e., 1.4 mAh cm⁻²; Figure 3b). In the following step, however, the sodiation was pushed to 3.5 mAh (i.e., 1.75 mAh cm⁻²), corresponding to 25% more than the intrinsic Na-BP capacity. The half-cell was then desodiated, sodiated, and desodiated again with a 3.5 mAh fixed capacity in each step. In agreement with the previous findings (Figure 1c), the sodiation occurs largely along a rather flat discharge plateau with an average voltage of about 0.13 V, corresponding to the formation of Na-BP in the anolyte, followed by a very flat voltage plateau at about -0.06 V, associated with the sodium metal plating on the Ni foam current collector. Upon the subsequent desodiation, the appearance of a flat voltage plateau at about 0.06 V indicates the reversible sodium metal stripping, followed by a sloped charge plateau with an average voltage of around 0.25 V associated to the Na-BP consumption to form biphenyl. The high reproducibility of the desodiation curves in Figure 3b, reveals the high reversibility of the overall Na-storage process. The two processes appear to be very well distinguishable with the voltage profile signatures of the Na-BP anolyte and the sodium plating/stripping being very well separated from each other. Remarkably, the “plating/stripping plateau” indicates that the Na-BP molecules may act as Na⁺ mediator/carrier for the plating/stripping process, indicating that the Na-BP anolyte can play the carrier role for both the Na-ions and electrons (Figure 3c).

To further test the possibility of realizing Na-metal-free anode cells (Ni foam|Na-BP|NASICON|seawater|carbon felt), the electrochemical processes occurring in the negative compartment during charge and discharge are

Charge:	Na ⁺ + BP (sol) + e ⁻ → Na-BP (sol)	followed by	Na ⁺ + e ⁻ → Na (s)
Discharge:	Na-BP (sol) → Na ⁺ + BP + e ⁻	followed by	Na (s) → Na ⁺ + e ⁻

while those occurring in the positive compartment are described above.

As demonstrated in Figure 4a, such a full-cell shows highly reversible cycling with a total capacity of 4.0 mAh (= 2.0 mAh cm⁻²).

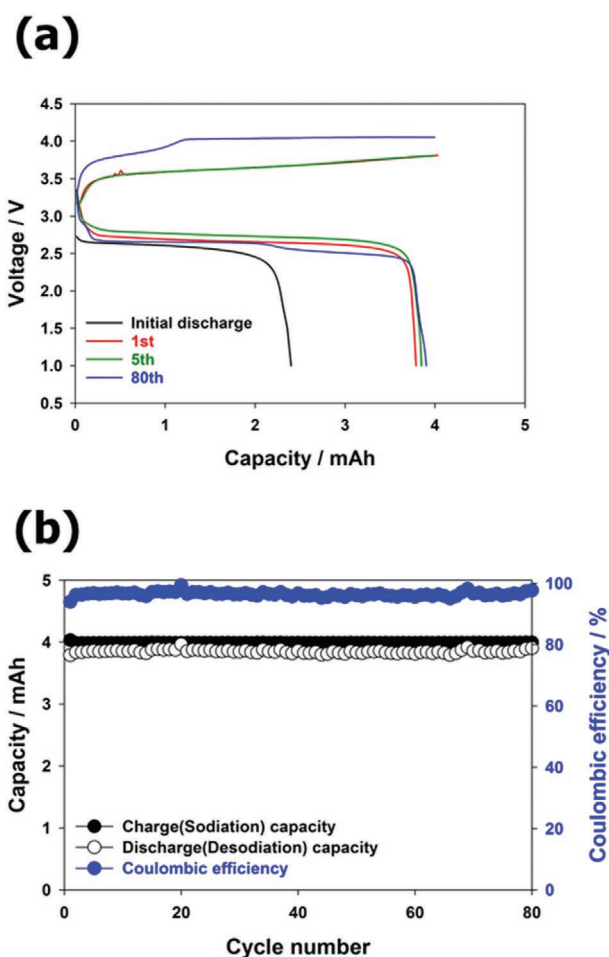


Figure 4. a) Galvanostatic dis-/charge profiles for a seawater battery-type full-cell employing Na-BP in DEGME as anolyte at a current density of 0.5 mA cm⁻² (discharge cut-off: 1.0 V). b) Electrochemical performance of the seawater battery-type full-cell, plotting the dis-/charge capacity and coulombic efficiency versus the cycle number (current density: 0.5 mA cm⁻²; see also (a) for the corresponding dis-/charge profiles for selected cycles).

In more detail, from the first discharge step, the capacity contributed by the Na-BP anolyte is determined to be 2.4 mAh (= 1.2 mAh cm⁻²). Upon the first charge the sodiation of the negative electrode is pushed to a total capacity of 4.0 mAh, with the extra capacity being achieved via the sodium metal plating on the Ni foam current collector of ≈1.6 mAh (i.e., 0.8 mAh cm⁻²). The slope of the voltage profiles upon charge of the cells appears more pronounced—presumably due to the concomitant overvoltage at the nonoptimized cathode current collector (the carbon felt). This is also indicated by the increase in polarization and the average coulombic efficiency of 96.5%, revealing the occurrence of some irreversible processes in the full-cell (Figure 4b). Nonetheless, the Na-BP anolyte has a highly advantageous impact on the full-cell cycling as compared to standard electrolytes such as 1 M NaOTf in TEGDME (Figure S2c, Supporting Information). Additionally, two rate performance tests were conducted to compare the Na-BP anolyte and the NaOTf-based reference anolyte. The first consisted in executing the polarization curve on two cells, each

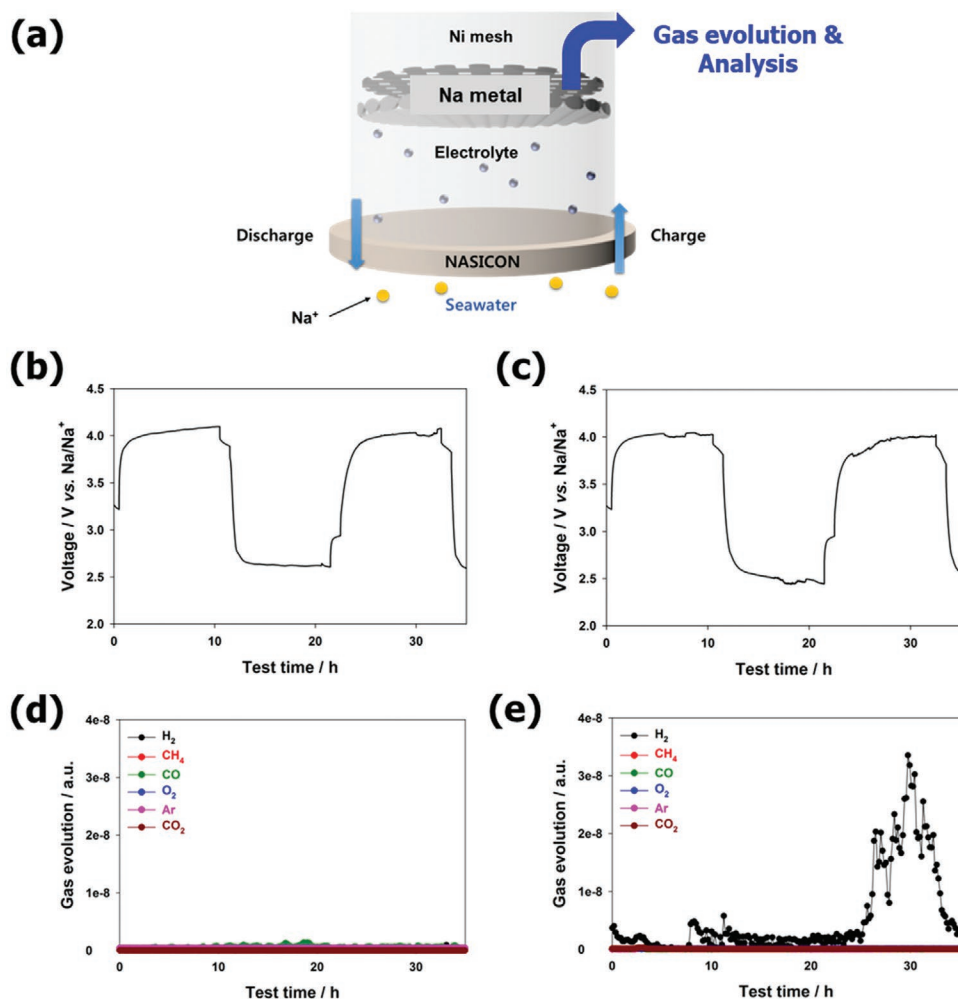


Figure 5. Comparative in situ DEMS analysis of Na|Na-BP|seawater and Na|NaOTF|seawater cells, applying a current density of 0.25 mA cm^{-2} for the charge and discharge (each 10 h). a) Schematic illustration of the cell setup for the DEMS analysis. b,c) The corresponding voltage profiles for the Na-BP and NaOTF comprising cells, respectively. d,e) The gas evolution occurring for the Na-BP and NaOTF containing cells, respectively.

containing one of the two anolytes, and sodium metal anode at a scan rate of 0.05 mA s^{-1} . As shown in Figure S3a of the Supporting Information, the Na-BP anolyte yields to a maximum output power of $\approx 5.4 \text{ mW cm}^{-2}$, which is higher than that of the NaOTF-based reference anolyte ($\approx 5 \text{ mW cm}^{-2}$). Also, the rate capability test of an anode-free, seawater cell employing the Na-BP anolyte was performed. As shown in Figure S3b of the Supporting Information, the Na-BP anolyte exhibits reversible and stable voltage profiles even under higher currents (from 1 to 3 mA). In fact, the Na-BP anolyte enables lower voltage hysteresis and higher capacities with higher reversibility (over 80 cycles in Figure 4b, and over 1000 h in Figure S4a, Supporting Information, and over 360 cycles in Figures S4b,c, Supporting Information, respectively) thanks to the sodium storage capability of the anolyte and its “mediating” function for the sodium metal plating and stripping (Figure 3c).

To further highlight the beneficial effects of Na-BP, a comparative differential electrochemical mass spectrometry (DEMS) analysis of the Na-BP anolyte and the NaOTF-based reference electrolyte was executed. The tests were performed in cells with a very similar design as the seawater full-cells

(Figure 5a). These cells were charged and discharged repeatedly (see Figure 5b,c) while detecting the gas formation in the negative compartment (see Figure 5d,e, respectively). As apparent from Figure 5d, the cell comprising the Na-BP anolyte does not show any significant gas evolution, while the cell containing the NaOTF-based electrolyte reveals a substantial hydrogen evolution—especially during the second charge (Figure 5e), which also explains the rather noisy voltage profile (Figure 5c). The formation of hydrogen is commonly assigned to the reaction of trace water with the sodium metal anode or, potentially, some decomposition of the electrolyte.^[13] The fact that the Na-BP containing cell does not show such a hydrogen evolution, thus, indicates a superior stability of the electrolyte and a potential H_2O -scavenging effect of the Na-BP molecules.^[10a] This effect was further confirmed by assembling flexible pouch-type cells for which the volume expansion due to gas formation can be easily followed by visual observation (although in a qualitative manner). Cycling these cells under the same experimental conditions used for the DEMS experiments, a substantially improved lifetime was observed for the cell comprising the Na-BP anolyte, while the cell containing the NaOTF-based

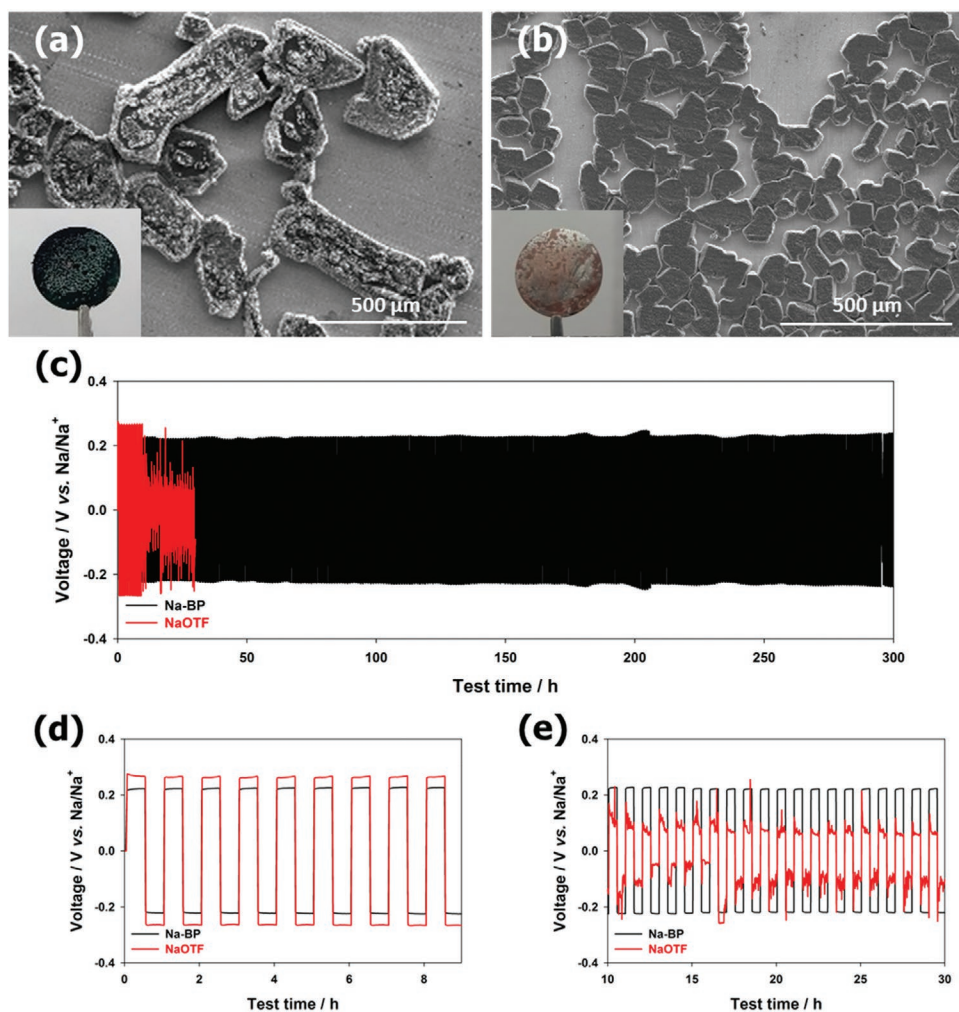


Figure 6. SEM images of Cu electrodes with plated Na metal, employing a) the Na-BP-based anolyte or b) 1 M NaOTF in TEGDME as electrolyte (current density: 0.25 mA cm^{-2} ; plating time: 6 h) with photographs of the corresponding electrodes as inset. c) Sodium stripping/plating experiments for symmetric Na|anolyte|electrolyte|NASICON|anolyte|electrolyte|Na cells employing either Na-BP in DEGME (in black) or 1 M NaOTF in TEGDME (in red) at a current density of 1 mA cm^{-2} with a stripped/plated capacity of 0.5 mAh cm^{-2} for each step. d,e) Magnification of the (d) initial and (e) following stripping/plating cycles upon the first 30 h of the experiment.

electrolyte faded after less than 17 cycles (Figure S5a, Supporting Information) due to the severe gas evolution and, hence, volume expansion of the cell (Figure S5b). The same did not occur for the cell employing the Na-BP anolyte.

An additional advantageous effect of the Na-BP anolyte is observed when studying the sodium metal deposition on Cu foil by means of ex situ scanning electron microscopy (SEM). In the case of Na-BP, the plated sodium metal grains are much larger in size (Figure 6a; Figure S6a, Supporting Information) compared to the Na metal grains obtained when using 1 M NaOTF in TEGDME (Figure 6b; Figure S6b, Supporting Information), suggesting that the nucleation barrier is lower in case of the NaOTF-based electrolyte which favors the deposition of rather small Na metal grains.^[14] The overpotential for the sodium metal deposition, however, is higher in case of the NaOTF-based electrolyte, as revealed by plating/stripping tests in symmetric Na|anolyte|electrolyte|NASICON|anolyte|electrolyte|Na cells (Figure 6c; this setup has been used to avoid

any potential short circuit in case of the electronically conductive Na-BP anolyte). For the NaOTF-based cell, it is about 270 mV compared to 220 mV for the Na-BP comprising cell for the initial 10 stripping/plating cycles (Figure 6d). While it subsequently remains essentially constant for the latter for several hundred hours, the cell with the NaOTF-based electrolyte is fading rapidly soon after (Figure 6c,e) and the voltage response becomes very unstable and noisy, indicating an unstable SEI and massive Na dendrite growth.^[4b] As a matter of the fact, the Na dendrite growth with the NaOTF-based electrolyte is clearly observed using an in-house developed, transparent quartz cell incorporating a sodium metal counter and working electrode (Figure S7a, Supporting Information). Upon the application of a constant current of 1.6 mA cm^{-2} , needle-like sodium dendrites have reached the opposite electrode after only 60 min, which resulted in the cell short circuit (see Figure S7b, Supporting Information, for a series of photographs to track the evolution of the needle-like dendrite growth).

Finally, one may add that the Na-BP anolyte, different from other highly concentrated anolyte/electrolyte systems, also provides a substantial cost advantage compared to, e.g., 1 M NaOTf in TEGDME, with a six times lower price when considering the cost of the given components (Figure S8, Supporting Information), thus, rendering this system highly promising for commercial applications.

3. Conclusion

Na-BP in DEGDME is a very powerful and cost-efficient anolyte system for sodium metal batteries like the seawater battery, given that an additional electronically insulating electrolyte layer is employed. Such an anolyte prevents hydrogen evolution, shows rather low sodium storage overpotentials, suppresses needle-like sodium dendrite growth, and allows for stable cycling of symmetric Na/Na cells and sodium–seawater battery full-cells. Remarkably, Na-BP does not only add to the capacity obtained by sodium metal deposition, but alters the dis-/charge mechanism by acting as a “mediator/carrier” for the sodium transport in the negative electrode compartment thanks to its simultaneous ionic and electronic conductivity. These results make it an ideal candidate for the realization of cost-efficient and long-term stable large-scale electrochemical energy storage devices.

4. Experimental Section

Preparation of Na-BP Solution: The Na-BP solution was prepared as it follows: DEGDME (Sigma-Aldrich, 99%) was dried over a molecular sieve (Samchun chemical, 4 Å, 8–12 mesh) to remove residual water for three days. Subsequently, biphenyl (BP; Sigma-Aldrich, 99.5%) was added into the dried DEGDME solvent to obtain a 1 M solution. The 1 M BP-DEGDME solution was stirred over 10 h before adding the corresponding molar amount of sodium metal (Acros Organics, 99.8%). This step includes a charge transfer reaction,^[15] resulting in the formation of the targeted alkali metal-biphenyl-ether solution (1 M Na-BP-DEGDME or Na-BP). To ensure the complete formation of Na-BP, additional Na metal (≈ 0.5 M) was added. The final Na concentration of the resulting solution was determined to be 1.1 M by means of inductively coupled plasma optical emission spectroscopy, herein referred to as saturated Na_{sat} -1 M BP-DEGDME. As the single components as well as the final solution are sensitive to water, all preparation steps were performed in a glove box with a H_2O and O_2 content of less than 1 ppm.

Physicochemical Characterization: The morphology of the Na metal plated on Cu foil was studied by ex situ SEM (Hitachi S-4800) and the elemental analysis was carried out by energy-dispersive X-ray spectroscopy. Prior to the analysis, the Cu electrodes were rinsed with 1,2-dimethoxyethane to remove the remaining anolyte/electrolyte.

Electrochemical Characterization: The electronic and ionic conductivity was determined using a portable conductivity meter (Eutech CON 150 Conductivity meter, EUTECH). For the half-cell tests, the Na-BP solution was employed as working electrode with Na metal serving as counter and reference electrode, separated by a NASICON ($\text{Na}_3\text{Zr}_2\text{Si}_2\text{PO}_{12}$) solid-state electrolyte (obtained from 4 TO ONE Energy). As nonaqueous electrolyte for the sodium metal electrode, 1 M sodium trifluoromethanesulfonate (NaOTf; Tokyo Chemical Industry, >98%) in TEGDME (Sigma-Aldrich, >99%) was used. The latter was dried over a molecular sieve for three days to remove residual water—just like the DEGDME utilized for the preparation of the Na-BP solution. Galvanostatic cycling was conducted on a WonATech WBCS 3000 battery

tester within a potential range of 0.0–1.0 V. For the SWB full-cells, natural seawater comprising about 0.47 M NaCl was employed as catholyte and a carbon felt (4×4 cm) served as current collector. 2465-type seawater coin cells and seawater flow cell testers were supplied by 4 TO ONE Energy. For a comparative investigation, the Na-BP solution was used either as “liquid anode” or as anolyte in combination with Na metal. Galvanostatic cycling was performed by charging the cells to a certain capacity cut-off and discharging it to a voltage cut-off of 2.0 V (in case of the “liquid anode”) or 1.0 V (in case of the Na-BP anolyte in combination with sodium metal). ITIC measurements were conducted to differentiate between the ionic and electronic conductivity, applying a constant voltage of 0.1 V. The resulting currents related to the ionic and electronic conductivity were measured for 1 h using a Biologic VSP-300 potentiostat. EIS was conducted using the same potentiostat. Symmetric Na|electrolyte|NASICON|electrolyte|Na cells were subjected to plating/stripping tests at a current density of 1 mA cm^{-2} with a total capacity transfer of 0.5 mAh cm^{-2} . In situ DEMS cell analysis was used to monitor gas evolution applying a current density of 0.25 mA cm^{-2} for the charge and discharge (each 10 h). The gas evolution in the cell was probed in 10 min intervals. All cells were assembled in an argon-filled glove box with less than 1 ppm of both oxygen and moisture.

Supporting Information

Supporting Information is available from the Wiley Online Library or from the author.

Acknowledgements

Y.K., J.J., and H.Y. contributed equally to this work. This work was supported by the 2020 Research Fund (1.200070.01) of UNIST (Ulsan National Institute of Science and Technology). In addition, Y.K., G.-T.K., D.B., and S.P. would like to acknowledge financial support by the Helmholtz Association.

Conflict of Interest

The authors declare no conflict of interest.

Keywords

anolytes, liquid anodes, seawater batteries, sodium biphenyl, sodium metal anodes

Received: February 10, 2020

Revised: March 15, 2020

Published online:

- [1] S. Chu, Y. Cui, N. Liu, *Nat. Mater.* **2017**, *16*, 16.
- [2] a) B. Dunn, H. Kamath, J.-M. Tarascon, *Science* **2011**, *334*, 928; b) H. Chen, T. N. Cong, W. Yang, C. Tan, Y. Li, Y. Ding, *Prog. Mater. Sci.* **2009**, *19*, 291.
- [3] D. Bresser, S. Passerini, *Power Engineering: Advances and Challenges Part B: Electrical Power* (Eds: V. Badescu, G. C. Lazaroiu, L. Barelli), CRC Press, FL, USA **2018**, Ch. 5.
- [4] a) X. Zheng, C. Bommier, W. Luo, L. Jiang, Y. Hao, Y. Huang, *Energy Storage Mater.* **2019**, *16*, 6; b) B. Lee, E. Paek, D. Mitlin, S. W. Lee, *Chem. Rev.* **2019**, *119*, 5416.

- [5] a) J.-K. Kim, F. Mueller, H. Kim, D. Bresser, J.-S. Park, D.-H. Lim, G.-T. Kim, S. Passerini, Y. Kim, *NPG Asia Mater.* **2014**, *6*, e144; b) S. M. Hwang, J.-S. Park, Y. Kim, W. Go, J. Han, Y. Kim, Y. Kim, *Adv. Mater.* **2019**, *31*, 1804936. c) S. T. Senthilkumar, W. Go, J. Han, L. P. T. Thuy, K. Kishor, Y. Kim, Y. Kim, *J. Mater. Chem. A* **2019**, *7*, 22803; d) P. K. Shen, A. C. C. Tseung, C. Kuo, *J. Power Sources* **1994**, *47*, 119; e) W. S. Wilcock, P. C. Kauffman, *J. Power Sources* **1997**, *66*, 71; f) W. Zhang, W. Chen, X. Zhao, Q. Dang, Y. Li, T. Shen, F. Wu, L. Tang, H. Jiang, M. Hu, *Angew. Chem., Int. Ed.* **2019**, *58*, 7431.
- [6] Y. Kim, S. M. Hwang, H. Yu, Y. Kim, *J. Mater. Chem. A* **2018**, *6*, 3046.
- [7] H. Wang, D. Yu, C. Kuang, L. Cheng, W. Li, X. Feng, Z. Zhang, X. Zhang, Y. Zhang, *Chem* **2019**, *5*, 313.
- [8] F. Han, A. S. Westover, J. Yue, X. Fan, F. Wang, M. Chi, D. N. Leonard, N. J. Dudney, H. Wang, C. Wang, *Nat. Energy* **2019**, *4*, 187.
- [9] a) Y. Sun, L. Zhao, H. Pan, X. Lu, L. Gu, Y.-S. Hu, H. Li, M. Armand, Y. Ikuhara, L. Chen, X. Huang, *Nat. Commun.* **2013**, *4*, 1870; b) Y. Wang, X. Yu, S. Xu, J. Bai, R. Xiao, Y.-S. Hu, H. Li, X.-Q. Yang, L. Chen, X. Huang, *Nat. Commun.* **2013**, *4*, 2365.
- [10] a) J. Yu, Y.-S. Hu, F. Pan, Z. Zhang, Q. Wang, H. Li, X. Huang, L. Chen, *Nat. Commun.* **2017**, *8*, 14629; b) F. Liang, X. Qiu, Q. Zhang, Y. Kang, A. Koo, K. Hayashi, K. Chen, D. Xue, K. N. Hui, H. Yadegari, X. Sun, *Nano Energy* **2018**, *49*, 574; c) S. T. Senthilkumar, H. Bae, J. Han, Y. Kim, *Angew. Chem., Int. Ed.* **2018**, *57*, 5335.
- [11] a) H. Pan, X. Lu, X. Yu, Y.-S. Hu, H. Li, X.-Q. Yang, L. Chen, *Adv. Energy Mater.* **2013**, *3*, 1186; b) G. Chu, B.-N. Liu, F. Luo, W.-J. Li, H. Lu, L.-Q. Chen, H. Li, *Chin. Phys. B* **2017**, *26*, 078201.
- [12] H. Kim, J.-S. Park, S. H. Sahgong, S. Park, J.-K. Kim, Y. Kim, *J. Mater. Chem. A* **2014**, *2*, 19584.
- [13] a) A. Bhide, J. Hofmann, A. Katharina Dürr, J. Janek, P. Adelhelm, *Phys. Chem. Chem. Phys.* **2014**, *16*, 1987; b) A. Jozwiuk, B. B. Berkes, T. Weiß, H. Sommer, J. Janek, T. Brezesinski, *Energy Environ. Sci.* **2016**, *9*, 2603; c) Y. Lee, J. Lee, J. Lee, K. Kim, A. Cha, S. Kang, T. Wi, S. J. Kang, H.-W. Lee, N.-S. Choi, *ACS Appl. Mater. Interfaces* **2018**, *10*, 15270.
- [14] D. H. Kim, H. Choi, D. Y. Hwang, J. Park, K. S. Kim, S. Ahn, Y. Kim, S. K. Kwak, Y.-J. Yu, S. J. Kang, *J. Mater. Chem. A* **2018**, *6*, 19672.
- [15] a) F. Pan, J. Yang, C. Jia, H. Li, Q. Wang, *J. Energy Chem.* **2018**, *27*, 1362; b) S. V. Bondarchuk, M. Carrera, M. de la Viuda, A. Guijarro, *New J. Chem.* **2018**, *42*, 5168.